Numerical Assessment of Radiative Heat Transfer Impact on Pollutant Formation Processes in a Compression Ignition Engine

Filip Jurić[a]
e−mail: filip.juric@fsb.hr

Zvonimir Petranović[b]
e−mail: zvonimir.petranovic@avl.com

Milan Vujanović[*,a]
e−mail: milan.vujanovic@fsb.hr

Neven Duić[a]
e−mail: neven.duic@fsb.hr

[a] Faculty of Mechanical Engineering and Naval Architecture, University of Zagreb, Ivana Lučića 5, 10000 Zagreb, Croatia

[b] AVL AST List GmbH, Alte Poststraße 152, 8020 Graz, Austria

ABSTRACT

An imposed solution in the development process of compression ignition engines is the use of numerical research employing Computational Fluid Dynamics (CFD). At the high operating temperatures in compression ignition engines, the radiative heat transfer influences the overall temperature profile and heat transfer, which also affects the formation processes of pollutants. For the radiative transfer calculation in this work, method of discrete ordinates (DOM) employing Finite Volume Method (FVM) is implemented with user functions into the AVL FIRE™ CFD code. The absorptivity and emissivity are described with the implemented Weighted Sum of Grey Gases Model (WSGGM) based on non-isothermal and nonhomogeneous absorption coefficient correlations for carbon dioxide, water vapour and soot. The implemented procedure is extended to work with moving meshes, parallel computing and rezoning procedure, which are needed to account the radiative heat transport in internal combustion engines. Additionally, the focus of this work is on the performed validation of calculated mean temperature, pressure, rate of heat release and emission results against the compression ignition engine experimental measurements. Results with the implemented radiation model showed lower peak temperatures for approximately 10 K, which resulted in around 18 % lower nitrogen oxides concentrations, and up to 20 % higher soot concentrations at the end of engine operating cycle. The most

---
[*] Corresponding author

dominant impact of the radiative heat transfer on soot formation is visible at the crank angles, where peak temperatures occur. The performed parameter study of the piston and head wall emissivity values showed a reduction in mean in-cylinder pressure and NO mass fraction for a less reflective surface. From the conducted parameter analysis of ordinates number, the sufficient accuracy is achieved for simulations with eight ordinates, which resulted in approximately 50 % increased computational time. Finally, it may be concluded that the combination of implemented models is useful to predict the heat transfer of internal combustion engine focussing on the radiative heat transport, which can be an important factor for the development of forthcoming internal combustion engines.

KEYWORDS

Pollutant Emissions, Radiation, Engine, Participating Media

1. INTRODUCTION

Despite the development of new technologies in the transport and energy sector, most of the energy consumption is still provided by fuel consumption (Stančin et al., 2020). For this reason, the scientific investigations still aim to improve energy efficiency by controlling operation conditions, and adapt new more sustainable fuels to the existing energy systems (Bedoić et al., 2020) or additionally reduce the pollutants from conventional transport systems employing the new after-treatment technologies (Bešenić et al., 2020). The development and improvement of the combustion system is a great challenge that has been attempted to solve for many years (Mikulčić et al., 2020). The fossil fuel combustion process, as an exothermic process, is known to have a negative impact on the environment, and their reduction is crucial in the near future to reduce atmospheric pollution (Baleta et al., 2019). Currently, a significant source of harmful emissions is generated from gas turbines, internal combustion engines, industrial furnaces, and boilers, which still have room for improvement in current energy transition (Mikulčić et al., 2016). A promising approach for solving significant pollutant emissions is the utilisation of biofuels in conventional combustion systems, where the development of numerical models is of essential importance (Kun-Balog et al., 2017). Additional focus is also given on pollutants that are produced from the Internal Combustion (IC) engines, where the further developments of after-treatment, advanced combustion modelling, and alternative fuels are still ongoing (J Javier López et al., 2019). Recent researches investigated some unusual alternative fuels applicable for IC engine combustion such as from animal fat (Cernat et al., 2015), animal waste in leather industry (Lazaroiu et al., 2017) or methanol blends (Gupta and Mishra, 2019). An example of a modern approach for emission characteristics of a

compression ignition engine operated with biofuel blend is described in (Fajri et al., 2017). Contrarily, the current numerical research is providing solutions for improvement of the combustion process and engine efficiency, such as with the improvement of spray injection strategy (Sremec et al., 2017). Therefore, the combined approach of experimental research and Computational Fluid Dynamics (CFD) is utilised for more accurate calculation of temperature field inside combustion systems, that is a generator of pollutant formation processes (Bešenić et al., 2018). The employed CFD procedure in this work was performed for the analysis spray angle impact on combustion process in different piston design (Soni and Gupta, 2017). Fajri et al. utilise the CFD procedure for the determination of NO_x emissions from the compression ignition engines, where the emphasis was on the start of combustion and combustion duration of different fuel blends (Fajri et al., 2017). In (Lamas et al., 2019), authors showed the influence of injection strategy on emission results, where the reduction up to 30 % of NO_x emissions are achieved by the implementation of multi injection strategy. A promising solution for the determination of the NOx and soot emissions is a coupling of the CFD procedures with the neural networks to predict the emissions from different fuel blends as shown in (Taghavifar et al., 2016), where satisfactory prediction functions are achieved.

The additional complexity and computational demanding are the main reasons for not considering the impact of radiative heat transfer in IC engine numerical simulations (José J. López et al., 2019). With the development of the computational resources, the radiative heat transfer in the participating media can be approximated for the engineering applications. It is no longer sufficient not to include the impact of radiative heat transfer on pollutant formation processes to compute the amount of pollutant from IC engines (Paul et al., 2019). While the effect of radiation on the heat transfer in IC engines is in the most researches not considered, the radiation effect in the high-scale industrial application such as boilers and furnaces is commonly considered (Bohlooli Arkhazloo et al., 2019). Furthermore, the CFD procedure for calculating the radiative heat transport in jet engines is described in (Cerutti et al., 2008).

If the radiative heat transfer in participating media is assumed the Radiative Transfer Equation (RTE) needs to be solved. Approximated numerical models need to be employed in order to solve the RTE (Modest and Haworth, 2016). Among the many types of research on the topic of heat transfer by radiation in IC engines, just a few were carried out by solving the RTE (Benajes et al., 2015). All type of calculations that were conducted, where mainly using a Discrete Ordinate Method (DOM) radiative solver and the wide-band spectral model for calculating the absorption of the gas medium, including soot. The impact of radiative heat transfer and soot and NO_x formation process was investigated for the first time in the paper (Yoshikawa and Reitz, 2009), where the high values of absorption

coefficient inside the combustion chamber of the IC engine were achieved, due to the high soot concentrations and high-pressure. Although in small geometries, such as in passenger car IC engines, the impact of radiation on the whole heat transfer is not significant, the impact on the emission formation processes cannot still be ignored (Yildiz et al., 2019). It was evaluated, that the soot process formation depends greater on the radiation heat transfer in IC engines than the NO_x formation process (Fernandez et al., 2018). Numerical investigation of radiative heat transfer in IC engines employing DOM showed that radiation influences soot predictions by as much as 50 % (Yue and Reitz, 2019).

Of all the existing models, the DOM and its conservative modification Finite Volume Method (FVM) is the most utilised for calculation of radiative heat transfer in the CFD codes (Coelho, 2014a). That is why, for this analysis of radiative heat transfer in this work, the radiation model FVM is used, which can be applied for a wide range of industrial applications (Coelho, 2018). Nevertheless, the results on the IC engine with FVM radiation model have not been published briefly.

The DOM approximation, coupled with the conservative FVM, was implemented into the CFD software AVL FIRE™ in this work, based on the literature (Mishra et al., 2006). The implemented model considers all radiative heat transfer phenomena: absorption, emission, and scattering (Modest, 2013). The absorptivity and emissivity coefficients are calculated with the Weighted-Sum-of-Grey-Gases Model (WSGGM) base on non-isothermal and non-homogeneous correlations for H_2O and CO_2 mixtures in (Dorigon et al., 2013). With the development of exhaust particulate filters, the focus on soot modelling for the calculation of soot emissions in IC engines is no longer a priority (Guan et al., 2015). Although for the soot absorption coefficient modelling, it is essential to include the calculation of soot formation process, where the common correlation for soot modelling can be found in the (Cassol et al., 2015). The scattering phenomena can be neglected for the IC engine simulation, since it was neglected in all conducted IC engine calculations, due to the small size of soot particles and with an emissivity similar to grey gas model (Granate et al., 2016).

Furthermore, the algorithm for spatial angle discretisation with an arbitral number of theta and phi angles is implemented, where each spatial angle represents an ordinate. This algorithm is based on the procedure presented for regular geometries in the literature (Chai et al., 1994) and irregulated geometries (Chai et al., 1995). After Performing the spatial discretisation, the incident radiation can be calculated for each ordinate with corresponding transport equation, and then summarised in all ordinates to obtain the radiative source term in the energy conservation equation (Coelho, 2014b).

Since the radiative heat transfer directly influences the temperature field inside the combustion chamber, the numerical results of forming emission would also be affected by

4

the participating radiative media (Pang et al., 2016). The recent research for calculating emissions and optimising the combustion process by using the CFD in combustion chambers showed that the radiative properties of the gas inside the IC engine combustion chamber could not be neglected (Dec, 2009). For the definition of incident radiation at the boundary value, the implementation of symmetry, diffusive opaque and periodic boundary is performed for all ordinates directions based on the (Boulet et al., 2007). The implemented model is validated on simple geometry cases available in the literature. First validation case is parallel plates for which analytic result is available in (Fiveland, 1984), and the second one is the cylinder for which analytic result is available in (Dua and Ping, 1975). With the satisfactory agreement against the analytical results, the implemented radiation FVM DOM and radiative absorption coefficient model WSGGM are employed for IC simulations, where the combustion process is modelled with ECFM-3Z model as in (Jurić et al., 2019). Additionally, the results are compared with experimental measurements of the diesel engine from a production line passenger car, that were conducted by AVL GmbH.

According to the authors' knowledge, just a few papers are published regarding the CFD investigations of radiative heat transfer in internal combustion engines, and none of these has combined implemented models on an evaluation of compression ignition engine emissions and parameter study of wall emissivity factors, and spatial discretisation. Furthermore, the research revealed some new points regarding the impact of radiation on emission formation. The higher soot concentration influences the mean in-cylinder temperature during the combustion process and decreases the mean temperature during the combustion and expansion process of the IC engine. The regions of the highest soot concentration gradients showed the most significant difference in the temperature profiles between calculations that exclude and include the radiative heat transfer inside the engine combustion chamber. Additionally, the radiative heat transfer decreases the NO_x formation concentrations due to the overall lower in-cylinder temperatures. Obtain mean pressure, mean temperature, and heat release results are validated against the experiment. Finally, the implemented FVM DOM and WSGGM in combination with a combustion model in AVL FIRE™ are capable of numerical assessment of radiative heat transfer phenomena in IC engines and evaluation of its impact on the pollutant formation process.

2. MATHEMATICAL MODEL

In this section, the emphasis is on the mathematical modelling of the radiative heat transfer, where the implementation of the FVM DOM model is explained into details. All simulations in this work are calculated with Reynolds-Averaged Navier-Stokes (RANS) equations inside AVL FIRE™ v2019 CFD software. The Reynolds stress tensor is modelled by using the $k - \zeta - f$ turbulence model, which is considered as a suitable turbulence model

for modelling in compression ignition engines (Hanjalić et al., 2004), compared to the conventional $k - \varepsilon$ turbulence model described in (Honus et al., 2017). This model benefits with the robustness for modelling strong swirl motion and tolerance to a small value of dimensionless wall distance at the boundary cell-centre.

2.1. Spray modelling

In this work, Euler Lagrangian spray modelling approach is used, which assumes the liquid phase as parcels that move through continuum gas phase. Basic equations that describe the continuum phase are the conservation laws of mass, momentum and energy, which are calculated for the finite volumes. The motion of the liquid phase parcels is traced through the finite volume mesh by calculating their pathways, where the only observed force is drag force. The drag force is calculated by Schiller Neumman law, where the parcel trajectory is obtained from deceleration u_{pi} in the following term:

$$m_p \frac{du_{pi}}{dt} = 0.5\pi \, r^2 \rho C_D u_{rel}{}^2 \tag{1}$$

In Equation (1), the drag coefficient C_D is experimentally determined by the Cunningham correction factor. For the disintegration process of bulk liquid, WAVE disintegration model was employed. In such a model, liquid droplets or blobs are assumed to be spherical, and the increase of first perturbations on the surface of droplet is correlated to their wavelength (Gao et al., 2016).

The radius of the produced droplet, r_{stable} can be expressed as:

$$r_{stable} = \lambda_w C_1 u_{rel}{}^2 \tag{2}$$

where C_1 is the constant of WAVE model (assumed 0.61), λ_w is the wavelength on the droplet surface of the highest growing gradient. By using the WAVE model, the parcel size reduction rate is defined as:

$$\frac{dr}{dt} = -\frac{\lambda_w \, \Omega \, (r - r_{stable})}{3.726 \, r \, C_2} \tag{3}$$

The term C_2 in Equation (3) is a modelling constant which is used to delay the droplet breakup time, which varies from type of injector, and in this work is modelled as a constant value of 15. In the WAVE model, the wave growth rate Ω and the wavelength λ_w are calculated as depending on the local flow characteristics (Petranović et al., 2015). Evaporation process was described with Abramzon-Sirignano evaporation model (Abramzon and Sirignano, 1989), which assumes Le number value of evaporation process

6

1. Evaporation process and breakup disintegration process were modelled for sphere parcels of constant temperature and physical properties through fluid parcel, where the first injected parcels are assumed of same size as nozzle orifice diameter. For the wall parcel interaction a Walljet1 model is employed together with turbulent dispersion model, which details can be found in the literature (AVL AST GmbH, 2019).

2.2. Combustion modelling

For the combustion modelling, three-zones Extended Coherent Flame (ECFM-3Z) model is employed, which is appropriate for IC engine. ECFM-3Z features decoupled turbulence and chemistry calculation, for which standard species transport equation has to be solved (Colin and Benkenida, 2004).

$$\frac{\partial \overline{\rho}\tilde{y}_k}{\partial t} + \frac{\partial \overline{\rho}\tilde{u}_i\tilde{y}_k}{\partial x_i} - \frac{\partial}{\partial x_i}\left(\left(\frac{\mu}{Sc} + \frac{\mu_t}{Sc_t}\right)\frac{\partial \tilde{y}_k}{\partial x_i}\right) = \overline{\dot{\omega}_k} \tag{4}$$

where $\tilde{y}_k$ is the average mass ratio of specie k, and $\overline{\dot{\omega}_x}$ is the specie's source term from combustion reactions. For the mixture fraction f, fuel mass fraction y_{fu}, and residual gas mass g transport equations are determined (AVL AST GmbH, 2019):

$$\frac{\partial}{\partial t}(\rho y_{fu}) + \frac{\partial}{\partial x_i}(\rho \tilde{u}_i y_{fu}) = \frac{\partial}{\partial x_i}\left(\Gamma_{fu}\frac{\partial y_{fu}}{\partial x_i}\right) + S_{fu} \tag{5}$$

$$\frac{\partial}{\partial t}(\rho f) + \frac{\partial}{\partial x_i}(\rho \tilde{u}_i f) = \frac{\partial}{\partial x_i}\left(\Gamma_f \frac{\partial f}{\partial x_i}\right) \tag{6}$$

$$\frac{\partial}{\partial t}(\rho g) + \frac{\partial}{\partial x_i}(\rho \tilde{u}_i g) = \frac{\partial}{\partial x_i}\left(\Gamma_g \frac{\partial g}{\partial x_i}\right) \tag{7}$$
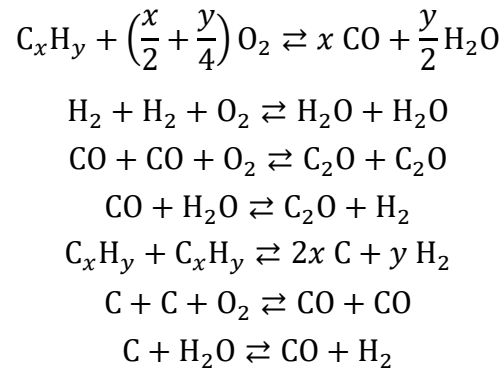
For the autoignition of air-fuel mixture the ignition delay and heat release are perambulated on the 0D reactors. The further model description of the model and calculation procedure of fuel mass ratio in flue gases, and mass fraction of fuel in the fresh air is described in literature (Jurić et al., 2019). The main limitation of the model is reduced chemistry kinetics, that is only account for the transport of standard species and that there is no unburnt fuel in the burnt gas phase (Mobasheri, 2015).

2.3. Emission modelling

The NO$_x$ emission formation in this work is modelled for prompt and thermal, employing the Extended Zeldovich model described in the literature (Vujanović et al., 2009). The Extended Zeldovich model also includes temperature fluctuations in its chemical

reactions employing probability density function with a two-moment function beta. The description of the Extended Zeldovich equations is described in (Petranović et al., 2016). Due to the high activation energy required to split the strong N_2 triple bond, the rate of formation of NO within this model is significant only at high temperatures (greater than 1800 K) (Rao and Honnery, 2013). Further NO_x modelling approaches can be found in the review paper (E et al., 2017).

The soot formation process is modelled with the reduced kinetic soot model, which is based on a detailed soot formation kinetic scheme (Pang et al., 2012). The reduced kinetic soot formation model incorporates seven gas phase reactions in the combustion model, with only one additional species for the soot (Wu et al., 2019). The reduced mechanism applied in this work is described with the following chemical reactions (AVL AST GmbH, 2019):

$$C_xH_y + \left(\frac{x}{2} + \frac{y}{4}\right)O_2 \rightleftarrows x\,CO + \frac{y}{2}H_2O$$

$$H_2 + H_2 + O_2 \rightleftarrows H_2O + H_2O$$

$$CO + CO + O_2 \rightleftarrows C_2O + C_2O$$

$$CO + H_2O \rightleftarrows C_2O + H_2$$

$$C_xH_y + C_xH_y \rightleftarrows 2x\,C + y\,H_2$$

$$C + C + O_2 \rightleftarrows CO + CO$$

$$C + H_2O \rightleftarrows CO + H_2$$

where C represents the soot. The reaction parameters for the primary soot formation reaction are changing with the air fuel ratio, while the presence of oxygen and water oxidizes the soot. The soot particle formation process is characterized by a gaseous-solid conversion, where the solid phase does not exhibit a uniform chemical and physical topology (AVL AST GmbH, 2019).

2.4. Radiative heat transfer modelling

The radiation in participating media is modelled by implementing DOM featuring FVM. The radiative heat transfer is consisting of three phenomena: absorption, emission and scattering. Figure 1 shows the scheme of incident radiation balance, where the media absorb the incoming radiation through participating media, enhanced by the emission of the media and scattered in different directions.
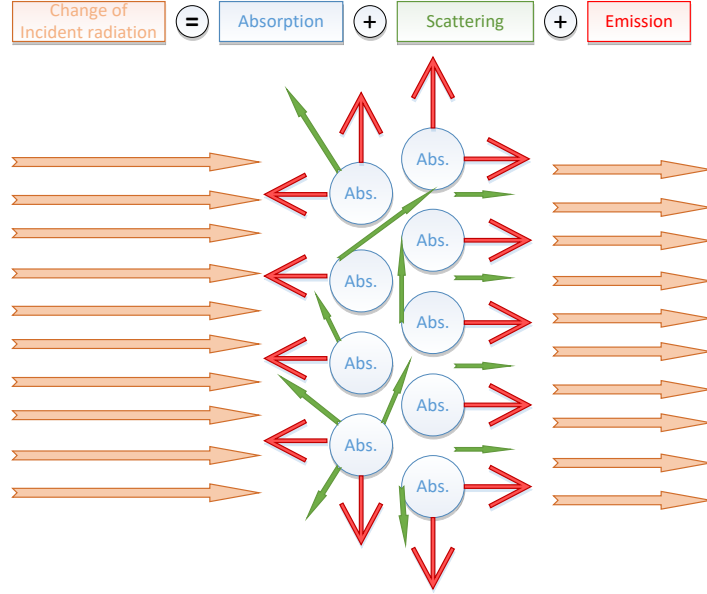
Figure 1   Scheme of radiative heat transfer in participating media

Such phenomena are specifed by the RTE, which in its full form can be written as

$$\frac{dI(\vec{r},\vec{s})}{ds} = \kappa(\vec{r})I_b(\vec{r}) - (\kappa + \sigma_s)(\vec{r})I(\vec{r},\vec{s}) + \frac{\sigma_s(\vec{r})}{4\pi}\int_{4\pi}I(\vec{r},\vec{s}')\Phi(\vec{r},\vec{s},\vec{s}')d\Omega' \tag{8}$$

which for the DOM featuring FVM gets the following expression for the spatial angle discretisation:

$$\frac{\partial I^l}{\partial s^l} = -(\kappa + \sigma_s)I^l + \kappa\left(\frac{\sigma T^4}{\pi}\right) + \frac{\sigma_s}{4\pi}\sum_{l=1}^{M}I^l\,\Phi^l\Delta\Omega^l \tag{9}$$

where I^l in the Equations (8) is the intensity of incident radiation in the l direction, κ is the absorption coefficient, σ_s is scattering coefficient, Φ is scattering phase function and s^l is an ordinate direction with its spatial angle $\Delta\Omega^l$. Spatial angle discretisation is showed in Figure 2, where the ordinate direction s^l is oriented perpendicular to its spatial angle.
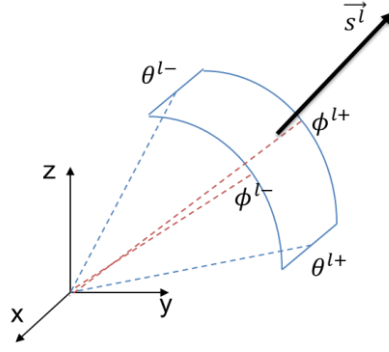
Figure 2　　Spatial angle discretisation

Equation (9) has to be solved for each discretised spatial angle, but the minimal number is recommended to be eight (Modest, 2013). When the intensity of incident radiation in each ordinate direction is obtained, the incident radiation is calculated as:

$$G = \sum_{i=1}^{n} I^l \cdot \Delta\Omega^l \tag{10}$$

where n is the total number of control angles (spatial angle discretisation). It can be noticed from Equation (9) that the incident radiation depends on the temperature. The interaction between the radiation heat transfer and the energy conservation equation for each cell in the computational domain is then modelled as the radiative heat source term in the energy conservation equation. The radiative source term is defined as:

$$S_{rad} = \kappa(G\text{-}4\sigma T^4) \tag{11}$$

which then is considered as an input in the source term of energy conservation equation. If Equation (9) is applied to the computational domain with three dimensional discretised cells, the following equation is obtained:

$$\sum_{i=1}^{\substack{\text{number of all cell faces}}} \Delta A_i \, I^l \int_{\Delta\Omega^l} \left(s^l_i \, n_i\right) d\Omega^l$$
$$= \left(\text{-}(\kappa + \sigma_s)I^l + \kappa\left(\frac{\sigma T^4}{\pi}\right) + \frac{\sigma_s}{4\pi} \sum_{k=1}^{\text{num\_dir}} I^k \, \Phi^k \Delta\Omega^k \right) \Delta\Omega^l \Delta V \tag{12}$$

The term on the left-hand side in Equation (12) presents the divergence of the incident radiation intensity, which can be affected by the three above mentioned phenomena. Equation (12) is calculated iteratively during the fluid flow iterations together with the fluid

10

flow calculation. The symmetry and diffusive opaque boundary conditions are implemented for the description of incident radiation in all ordinate's directions at the domain boundaries. The boundary condition for the diffusive walls is calculated only for the directions that are oriented into the computational domain and are calculated as (Coelho, 2013):

$$I_{bnd}^l = \varepsilon \frac{n_r^2 \sigma T^4}{\pi} + \frac{1-\varepsilon}{\pi} \sum_{(s^l \cdot n_i) < 0}^k I^k \cdot |n_i s_i| \Delta \Omega^k \tag{13}$$

where ε is the wall emissivity, and n_r is a refractive index which is for all surfaces in this work assumed one. The term on the left-hand side in Equation (13) represents the emission term, while on the right-hand side is the reflexion term. Diffusive reflection term is modelled as a reflection factor multiplied by the ratio between the radiation that hits the wall and geometrical characteristics of reflected directions.

The implemented algorithm for calculating spatial angle boundaries and directions is based on the upwind differencing scheme, and it is shown in Figure 3. Figure 3 shows how the intensities of incident radiation propagate in the computational domain with the global coordinate system.
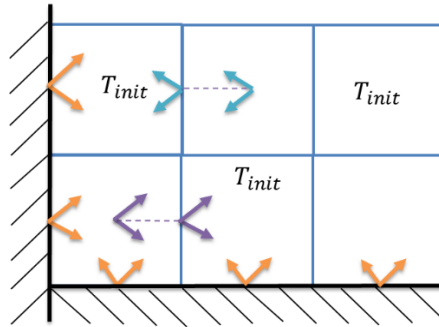

Figure 3   Algorithm for calculation of incident radiation.

Convergence criterium of Equation (11) is modelled with the following equation:

$$\frac{I_{new}^L - I_{old}^L}{I_{new}^L} < \text{convergence criterium} \tag{14}$$

For all calculations presented in this paper, convergence criterium was 0.001.

2.4.1. Absorption coefficient modelling

Absorption coefficient in this work is modelled by implemented WSGGM for grey gases, which is based on the CO_2 and H_2O correlations in the literature (Dorigon et al., 2013). The correlations in [13] model the soot absorption coefficient, added to the gas

absorption coefficient based on superposition rule of RTE. The following equation, where the calculate the total absorption coefficient κ_s presents the soot absorption coefficient:

$$\kappa = -\frac{\ln(1 - \varepsilon)}{s} + \kappa_s \tag{15}$$

The s in Equation (16) presents the thickness of absorption media, which is calculated by the following equation:

$$s = 3.6\frac{\Delta V}{A_{tot}} \tag{16}$$

where ΔV presents the cell volume and A_{tot} is the sum of all cell's faces. Emissivity ε in Equation (17) is calculated with the following equation of WSGGM:

$$\varepsilon = \sum_{i=0}^{2} \alpha_i \left(1 - e^{-a_i p s}\right) \tag{17}$$

where α_i is weight factor for the ith grey gas and is dependent only on temperature. The absorption coefficient a_i of the ith grey gas is determined by partial pressures p of the water vapour and carbon dioxide, which absorbs the incident radiation. For $i = 0$ the gas absorption coefficient has value α_o to resolve transparent windows in the spectrum between spectral regions of high absorption. For the transparent windows, the weight factor is calculated as:

$$\alpha_o = 1 - \sum_{i=0}^{2} \alpha_i \tag{18}$$

The other weighting factors are given by a polynomial of third order in the following form, where $b_{i,j}$ is the polynomial coefficient:

$$\alpha_i = \sum_{j=0}^{3} b_{i,j} T^j \tag{19}$$

The soot absorption coefficient is modelled as grey gas absorption, due to its the radiative properties, with the following equation:

12

$$\kappa_s = 0.672\,T\,c \qquad (20)$$

where c is the soot mass fraction.

2.4.2. Model Validation

Validation of the implemented model is conducted on simple geometry cases for which the analytical results exist, where the good agreement with analytical results is obtained. The validation is firstly conducted on parallel plates for which analytic result is available in (Fiveland, 1984). From the unidimensional solution, the case with the absorption coefficient $a = 0.1\ \mathrm{m}^{-1}$, and 1 m distance between two plates where the first plate is at 0 K and the second plate is at 2000 K. The numerical simulation is performed on 10x10x10 cells (1x1x1 m) cube mesh where the two opposing walls are set as black surface boundary conditions, where one plate does not emit any radiation due to its temperature 0 K. All remaining walls as symmetry boundary conditions, and the implemented FVM DOM was described with eight ordinates. Figure 4 shows the temperature field between two plates, where the good agreement with the implemented and the analytical result is achieved. For the second validation case, a cylinder of same height and diameter for which analytic result is available in (Dua and Ping, 1975) is selected. The cylinder has all walls assumed as black surfaces at 0 K, so there is not any emittance from cylinder walls. Only the absorption and emissivity of media at 500 K with absorption factor $a = 1\ \mathrm{m}^{-1}$ inside the cylinder is assumed. Figure 5 shows the result of the unidimensional wall heat flux at the cylinder base on cylinder hexahedron mesh with 20 cells in each direction. The good agreement with the analytical result is achieved. The more details about validation cases can be found in cited references.
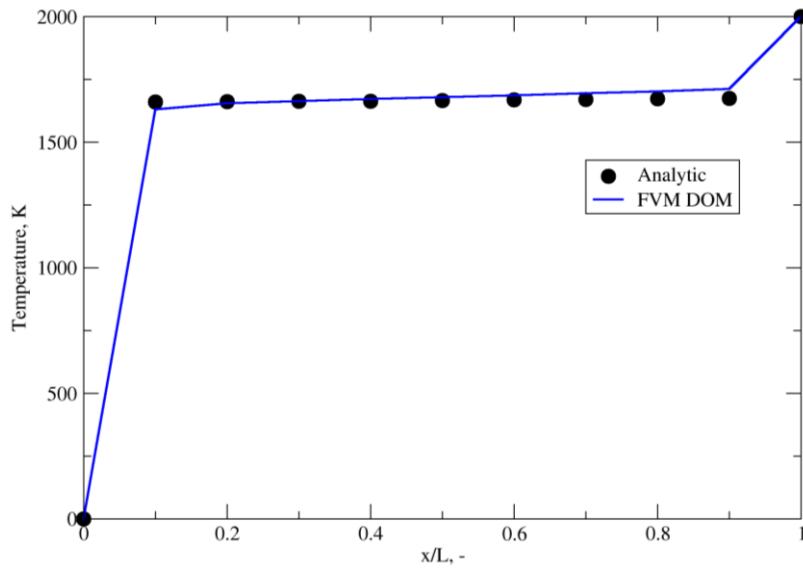

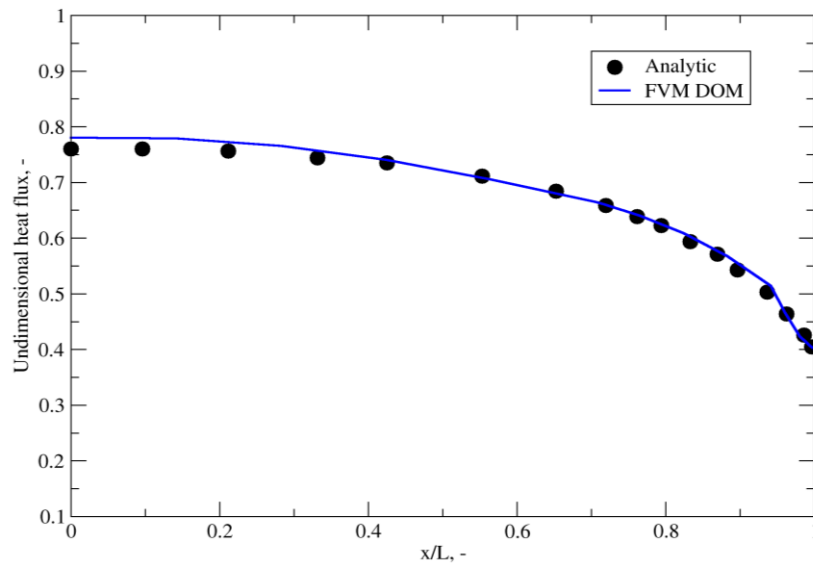Figure 4   Validation results for the parallel plates (Fiveland, 1984).

13

Figure 5 Validation results for cylinder case in (Dua and Ping, 1975).

3. EXPERIMENTAL DATA

The experimental measurements of the diesel engine from a production line passenger car are performed by AVL GmbH. The properties of the Volvo I5D engine and injection system are shown in Table 1.

Table 1   Engine and injection system specifications.

Type	Direct injection diesel
Bore (mm)	81
Compression ratio	16.5
Stroke (mm)	93.15
Spray Angle (°)	17.5
Number of nozzle holes	7
Diameter of nozzle hole (mm)	0.125

At the start of the experiment, the combustion chamber was initialised with a mixture of fresh air and Exhaust Gas Residuals (EGR) gas for each engine operating point. The injection temperature of the EN590 B7 fuel was set to 44°C, according to the experimental data.

The fuel inlet boundary condition was determined from the experimentally measured rate of injection, as shown in Figure 6. The rate of injection curve is given in non-dimensional parameters where the integral of the curve must be equalised with the injected liquid mass to obtain the injection velocity profile.
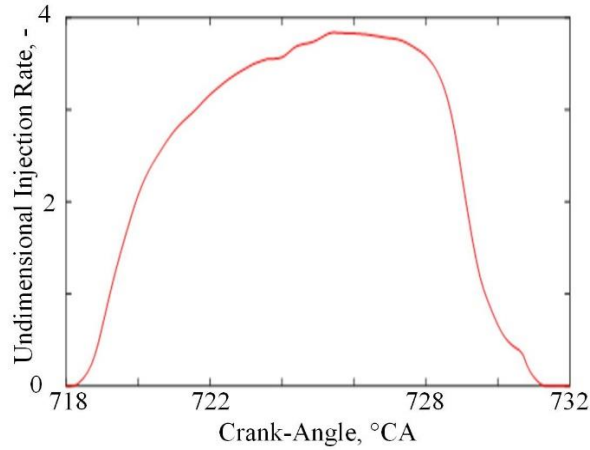
Figure 6   Injection rate profile.

4. NUMERICAL SETUP

Numerical calculations are performed with CFD code AVL FIRE^{TM}. The simulation time was set to the high-pressure cycle period when the inlet and exhaust valves are closed, particularly from 585°CA to 855°CA. Only the injection process from one nozzle hole is observed, and symmetric in-cylinder behaviour was assumed. During the calculation, a 1/7th segment of the complete engine cylinder was modelled, and the cyclic boundary conditions at the side surfaces were applied. The moving mesh was generated by the AVL FIRE^{TM} ESE DIESEL, and it contains around 35000 control volumes at the Top Dead Centre (TDC), and around 86000 cells in the Bottom Dead Centre (BDC). The generated computational domain with the defined boundary conditions, located at the TDC is shown in Figure 7. The mesh was generated with a 2-cell boundary layer, and in combination with wall functions, it was used to consider the wall impact on the fluid flow. The cylinder geometry is symmetric around the cylinder axis, and therefore, the cyclic (periodic) boundary conditions are applied at the sides. Mesh movement was described by rezoning procedure, where the meshes with the different number of cells, but same boundary conditions are exchanged during the compression and expansion (Tatschl, 2012). A compensation volume was added at the piston geometry to compensate geometry irregularities, and to conserve the exact compression ratio.
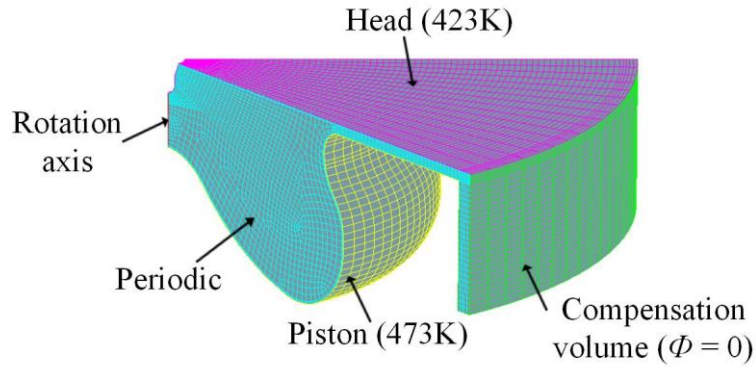
Figure 7   Computational domain positioned in the top dead centre.

Two additional meshes with smaller cell size, but with the same structure of block cells were generated in order to prove independency of the mesh on simulation results. The results on three meshes showed good agreement for mean in-cylinder pressure, temperature and Rate of Heat Release (RoHR) results, but also for the emission results.

For the mass conservation equation, the central differencing scheme is employed, while for the energy and turbulence conservation equations the upwind differencing scheme is applied. For the momentum equation, a combination of central differencing scheme and upwind differencing scheme was proposed by introducing a blending factor of 0.5. The convergence criteria for the solution are defined when the normalised pressure, momentum and energy residuals reach values lower than 10^{-4}. For turbulence and energy, the first order transport equations are solved using the upwind differencing scheme, while the central differencing scheme was employed for the mass conservation equation. The wall selections were defined as isothermal walls, and the air and fuel entrainments were prescribed with a constant temperature mass flow. All results showed in this work considered a maximum of 10 DOM FVM solver iterations, which were enough to achieve convergence. It was noticed, that the incident radiation results do not change significantly through each fluid flow iteration, and therefore the results calculated when the radiation solver is called each fluid flow iteration were compared when the solver was called every fifth and every tenth iteration. The results showed the approximately same values of mean pressure and pollutant mass fractions for all calculated incident radiations with every fluid flow iteration, every fifth and every tenth iteration. As a result, all simulations performed in this paper will be considered the calculation of incident radiation every tenth fluid flow iteration.

Selected ECFM-3Z combustion model parameters were extinction temperature at 200 K, autoignition time factor at the value of 1 and mixing parameter at the value of 1.

Operating points that are investigated in this paper feature a single injection, with the swirling motion inside the cylinder was defined as motion around symmetry axis with a value of 4740 min^{-1}, according to the experimental research. The initial conditions, combustion parameter and initial gas composition are shown in Table 2, where Case *a* and Case *b* are defined. The only differences between Case *a* and Case *b* is in the EGR mass fraction at the initial stage of the combustion, and initial temperature. From the initial conditions in Table 2, it is expected that Case *a* which features higher values of initial temperature and higher EGR mass fraction will show a more significant influence of radiative heat transfer than Case *b*. Both operating cycles have constant rotation speed and the same amount of injected fuel, for which the liquid properties of diesel EN590 B7 fuel are employed. The initial values of turbulent length scale and turbulent kinetic energy are estimated as 2 mm and 10 m^{2}s^2 following the setup presented in (Barbouchi and Bessrour, 2009).

Table 2   Initial conditions.

Operating point		Gas composition (kg/kg)	Case *a*	Case *b*
Engine speed (rpm)	2000	O_2	0.184638	0.2290
Number of injections	1	N_2	0.758305	0.7672
Injected mass (mg)	4.1	CO_2	0.03888	0.0331
Pressure (Pa)	210000	H_2O	0.01818	0.0155
		Temperature (K)	419	365

Numerical simulations were performed on Intel® Xeon® E5-2650 v4 @ 2.20 GHz which has 24 CPUs.

5. RESULTS AND DISCUSSION

In this section, important specific objectives, the major results, and the most significant conclusions of the paper are discussed. Firstly, the mean pressure, temperature and RoHR results for cases in Table 2 are presented, following with emission results. Finally, the parameter analysis of the piston and head emissivity factor is conducted and shown.

Figure 8 shows a comparison between temperature profile for the Case *a*, where the orange curve represents the results obtained for the numerical calculation without considering the radiative heat transfer, and the blue curve represents the results employing FVM DOM radiation model. The discrepancy between simulations with and without included radiation can be attributed mainly to the soot absorption, which has grey gas behaviour, that absorbs a high percentage of incident radiation in the high-temperature regions. The RoHR results (for the only 1/7th of the cylinder) shows a similar effect, where the energy loss due to the radiation is dominant for the highest RoHR values.
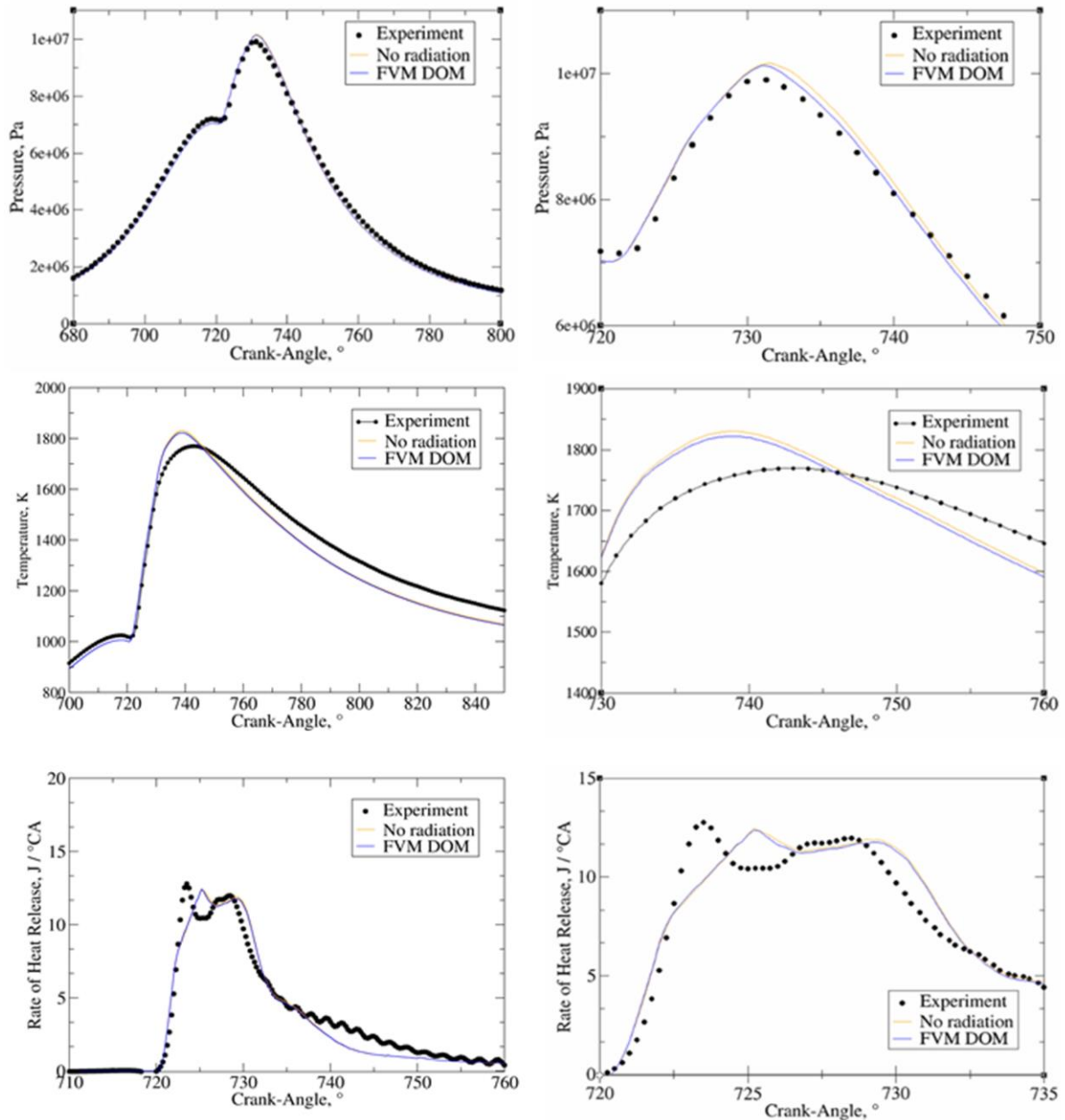
17

Figure 8   Case *a*: Mean pressure, temperature and rate of heat release curves for the results without considering radiative heat transfer and with FVM DOM (zoomed diagrams on right)

Figure 9 shows similar phenomena as Figure 8, but for the case without Exhaust Gas Recirculation in the initial phase of the operating point. The pressure curves of both operating conditions are in a good agreement with experimental results, but for Case *b* better agreement with the temperature results is achieved. The smaller discrepancy between result without radiation and with FVM can be attributed to the lower initial concentrations of CO_2 and H_2O, and the higher oxidising temperature of soot, due to better air to fuel ratio.
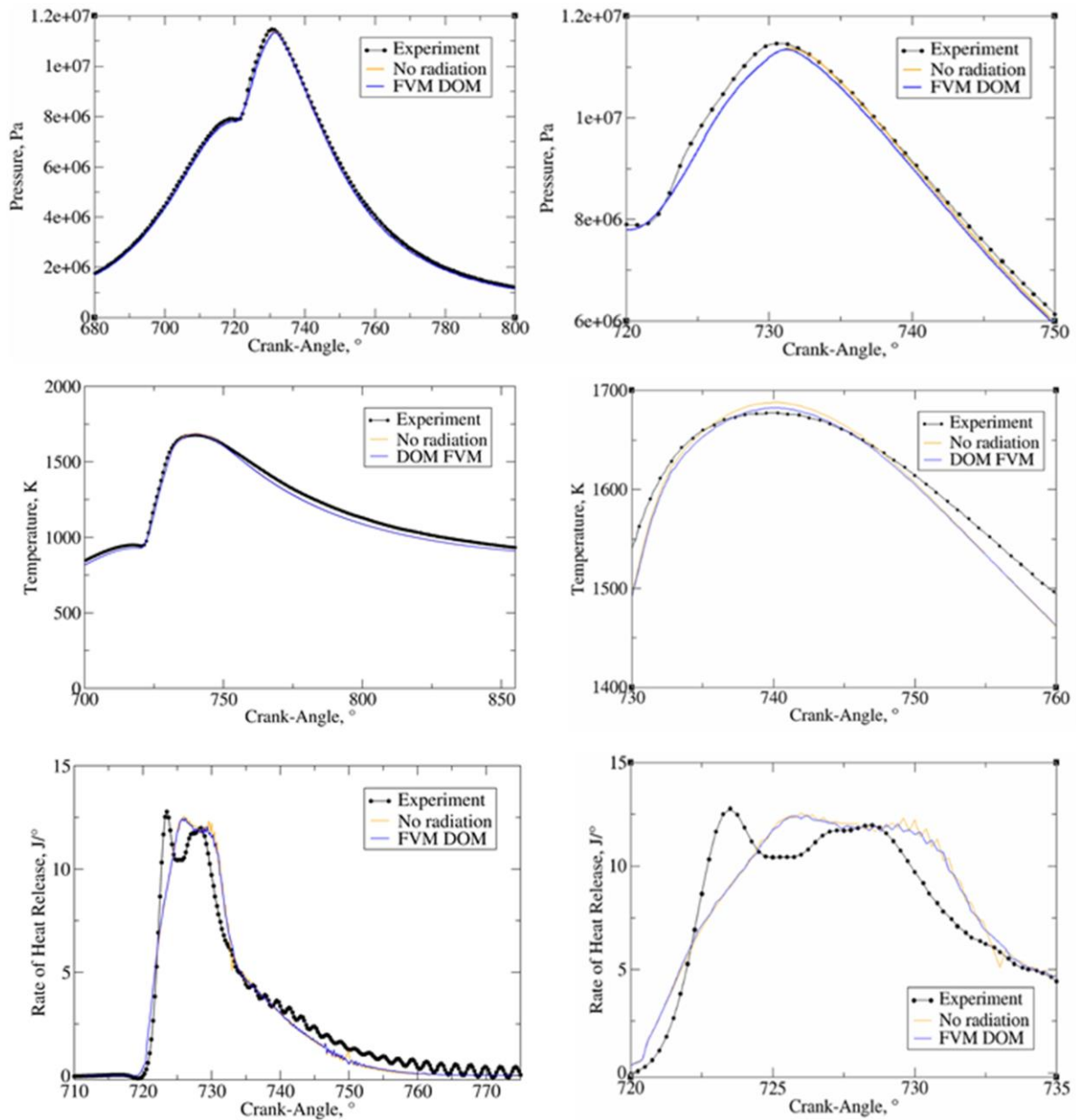
18

Figure 9   Case *b*: Mean pressure, temperature and rate of heat release curves for the results without considering radiative heat transfer and with FVM DOM (zoomed diagrams on right)

In both cases calculated RoHR curves underachieve the peak of firstly combusted regions and slightly postpone the combustion process. Although the same injected amount of fuel in both operating cases, significantly increased soot mass fraction at the end of the operating cycle is achieved in Case *a*, due to the lower initial oxygen concentrations. The difference between calculations without radiation and with the FVM DOM in Case *a* and Case *b* is mainly generated by soot concentrations inside the cylinder. Consequently, the higher soot concentrations in Case *a* resulted in a greater discrepancy between calculations without radiation and with the FVM DOM than in Case *b*.

19

Figure 10 shows 3D temperature profiles, where on the left side of diagram is the temperature field at the maximum soot mass fraction (740 °CA) for the simulation without radiation. On the right side is the temperature field for the included radiation. The highest difference between peak local temperature values for simulation without included radiation and with DOM FVM is around 15 K. Some discrepancy in temperature profiles is noticeable at the regions of high soot concentrations, which are also showed for 740 °CA in Figure 11. In the middle of the high-temperature region shown in Figure 10, the discrepancy between simulations is visible, which can be assigned to the H_2O and CO_2 absorption, since this region feature low values of soot mass fraction. Furthermore, CO_2 and H_2O as products of the combustion process are the most dominant exactly in the mentioned region where the first ignition is expected to occur. Figure 11 shows soot mass fraction profile inside the internal combustion engine, where the highest discrepancy between simulation without radiation and with FVM DOM is visible in the regions of highest temperature gradients. The distribution of soot mass fraction in Figure 11 shows a good agreement, where the regions of highest and lowest soot concentrations are preserved in calculations with and without radiative heat transfer. The total difference of soot mass fraction is achieved approximately 20 % higher with the calculations with FVM DOM than without considering radiation. Such a difference can have a great deal in the development process of new IC engines.
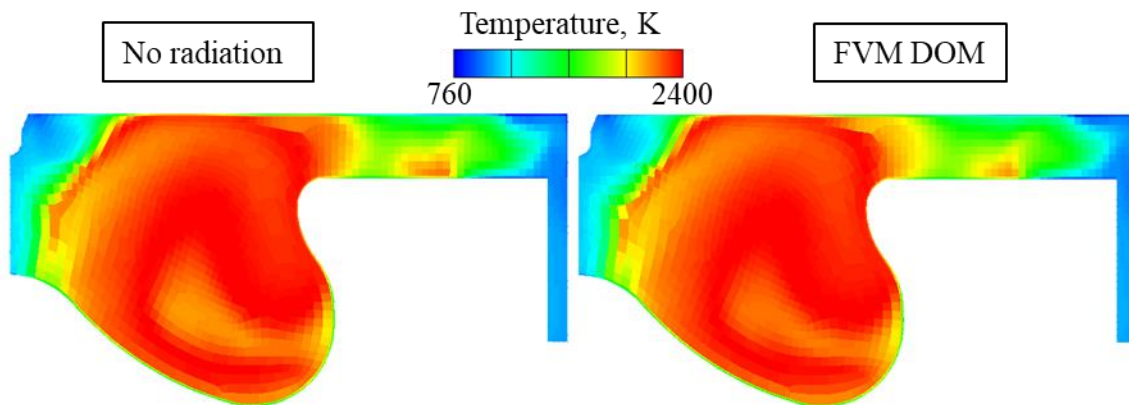

Figure 10   Temperature field for simulation without radiative heat transfer and with DOM FVM
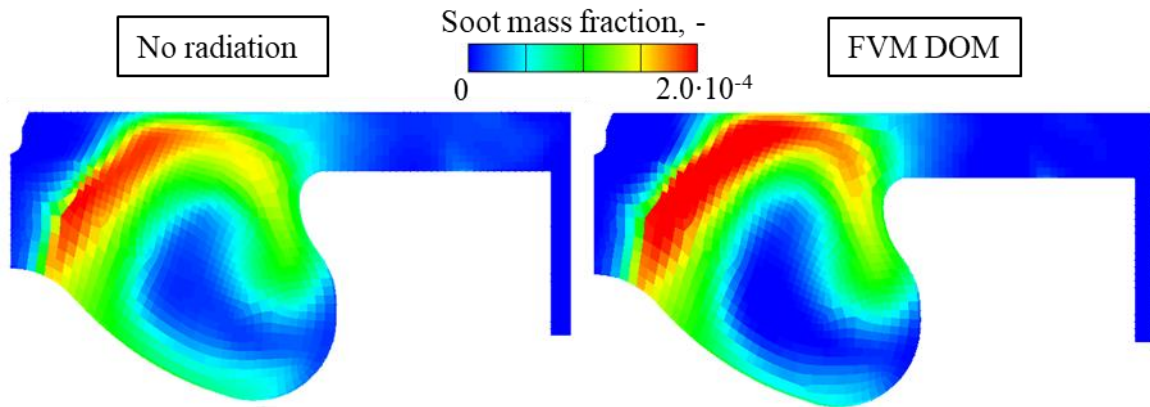
Figure 11   Soot mass fraction for simulation without radiative heat transfer and with FVM
DOM

Table 3 shows the emission results for both operating conditions, where the more significant difference between simulations without radiation and with FVM DOM is achieved in Case *a*, due to the higher EGR value. Additionally, in both cases, the trend in emission formation is that the NO emissions are decreased with included radiative heat transfer, which can be ascribed to the lower temperature results, while the soot emissions are increased with the included radiative heat transfer, due to the lower temperature of in-cylinder gas that promotes the oxidation process of the soot.

Table 3   NO and soot emission results at the exhaust manifold.

Operating point		Experiment	No radiation	With radiation
Case *a*	NO mass fraction, ppm	136	367	317
	Soot mass fraction, ppm	36.6	29.7	37.3
Case *b*	NO mass fraction, ppm	252	621	508
	Soot mass fraction, ppm	2.1	0.89	0.91

In Table 6, the comparison of calculation time between simulations with and without radiation is shown, where the approximately 50 % more time consuming are the simulations when the radiative heat transfer is calculating.

Table 4   World clock computational time for simulations with and without radiation
performed with 1 and 20 Central Processing Units (CPUs)

Number of CPUs	No radiation	With radiation
1	2 hours	3.5 hours
20	24 minutes	36 minutes

5.1. Parameter analyses

Impact of ordinates numbers on mean pressure during the operating cycle for eight, sixteen and thirty-two ordinates in Case *a* are shown in Figure 12. Each ordinate represents an additional direction for which the incident radiation is calculated, and for which an additional transport equation is calculated. As a result, the calculation with a higher number of ordinates have a numerically more accurate result but at the cost of higher computational demand. In Table 5, the world clock time of calculation time for simulations with eight, sixteen and thirty-two ordinates are shown, where an approximately linear increase in computational time is present with an increasing number of directions. It can be stated that for the calculation of radiative heat transfer in the IC engine 8 directions are enough to estimate the radiative impact on overall heat transfer.
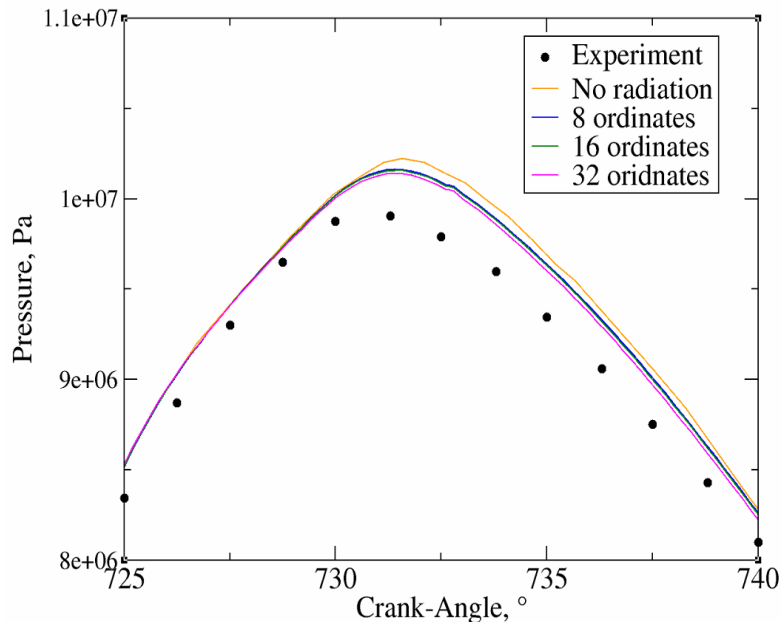

Figure 12   Mean pressure results for different number of ordinates

Table 5   World clock time for different number of ordinates in Case *a*

	Time, min
No radiation	24
8 ordinates	36
16 ordinates	49
32 ordinates	70

Figure 13 shows results obtained for the different values head and piston of the emissivity factor. Since the equivalent emissivity factor of the head and piston surface of

22

the experimental engine was not known, a parameter study was performed. The largest difference in mean pressure values can be noticed at the peak pressure values, which can be attributed to the highest temperatures at which the radiative heat transfer is more pronounced. Higher values of incident radiation filed inside the computational domain are achieved for the lower values of wall emissivity since the most of upcoming radiation is reflected into the domain, which results in higher incident radiation values at the piston and head selections. In all radiative heat transfer researches conducted in IC engine, a black surface emissivity was assumed. From Figure 13 it can be observed that with a lower emissivity, a better agreement with experimental results can be obtained, that can be attributed to metal surfaces in the experimental combustion chamber. Table 6 shows the impact of the piston and head emissivity values on exhaust emissions on Case *a* results, where a good trend in reducing of NO emissions can be attributed to the lower mean temperature inside the combustion chamber, that was observed in Figure 13. For the soot emissions, the higher soot mass fractions are achieved with lower emissivity values of head and piston wall.
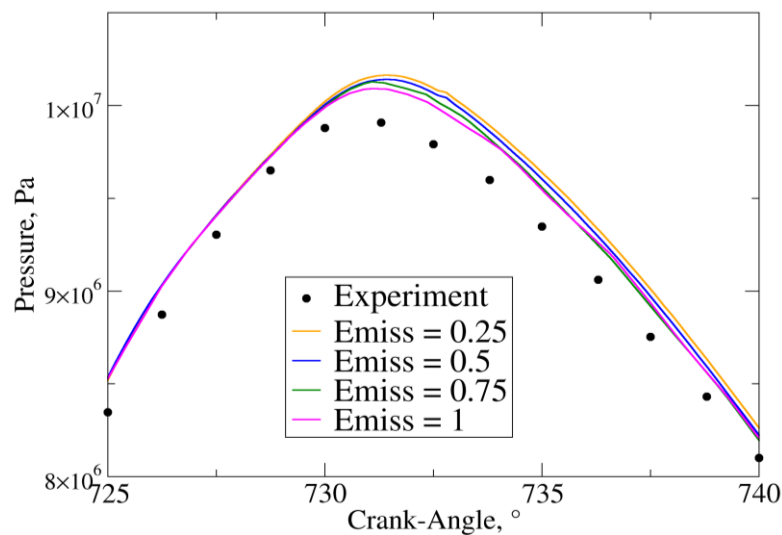

Figure 13   Mean pressure results for the different values of piston and head emissivity factors

Table 6   Impact of the piston and head emissivity factors on pollutant results at the end of Case *a*

	NO mass fraction, ppm	Soot mass fraction, ppm
Experiment	136	36.6
No radiation	367	29.7
Emissivity = 1	317	37.3
Emissivity = 0.75	316	37.8
Emissivity = 0.5	311	38.2
Emissivity = 0.25	301	39.2

6. CONCLUSIONS

The utilisation of the CFD for energy efficiency improvements and reduction of pollutant emissions in the industrial applications provides a valuable tool which provides feasibility to investigate different engine operating and design parameters. Discrete Ordinates Method employing Finite Volume Method is implemented by user functions into the AVL FIRE™ CFD software package. For the calculation of radiative absorption coefficient of participating radiative media, the implemented Weighted-Sum-of-Grey-Gases Model is employed featuring non-isothermal and non-homogeneous polynomial functions for H_2O, CO_2 and soot. The calculation procedure is adapted for computing on parallel units, rezoning process, and moving meshes, that are needed for calculation of IC engines. The validation of the implemented model on simple geometry cases showed a satisfactory agreement with the analytical results. After performed validation, the study was focused on the radiative heat transfer modelling in combination with the combustion process inside a diesel combustion chamber. Calculated mean pressure, mean temperature and the rate of heat release showed an agreement with the experimental traces. The most dominant impact on the radiative heat transfer is visible for the crank angles where the highest temperatures are achieved. The difference between calculations without radiation and with the FVM DOM in presented operating cases is mainly generated by soot concentrations in the regions of highest temperature gradients, where approximately 20 % lower total soot mass fraction is achieved with the simulations that account the radiative heat transfer. Parameter study of the piston and head wall emissivity values showed a reduction in mean in-cylinder pressure and NO mass fraction for a less reflective surface. The results obtained with the implemented radiation model predict lower peak temperatures for approximately 10 K, while the NO concentrations are decreased by 18 %, and soot concentration increased up to 20 %. From the conducted parameter analysis of ordinates number, the sufficient accuracy is achieved for simulations with eight ordinates, which resulted in approximately 50 % increased computational time. Finally, it can be concluded that if the additional physic phenomenon of radiative heat transfer is included in numerical simulations, a more accurate combustion and emission results are expected.

REFERENCES

Abramzon, B., Sirignano, W.A., 1989. Droplet vaporization model for spray combustion calculations. Int. J. Heat Mass Transf. 32, 1605–1618. https://doi.org/10.1016/0017-9310(89)90043-4

AVL AST GmbH, 2019. FIRE Documentation v2019.

Baleta, J., Mikulčić, H., Klemeš, J.J., Urbaniec, K., Duić, N., 2019. Integration of energy, water and environmental systems for a sustainable development. J. Clean. Prod. https://doi.org/10.1016/j.jclepro.2019.01.035

Barbouchi, Z., Bessrour, J., 2009. Turbulence study in the internal combustion engine 1, 194–202.

Bedoić, R., Jurić, F., Ćosić, B., Pukšec, T., Čuček, L., Duić, N., 2020. Beyond energy crops and subsidised electricity – A study on sustainable biogas production and utilisation in advanced energy markets. Energy 201. https://doi.org/10.1016/j.energy.2020.117651

Benajes, J., Martin, J., Garcia, A., Villalta, D., Warey, A., Domenech, V., Vassallo, A., 2015. An Investigation of Radiation Heat Transfer in a Light-Duty Diesel Engine. SAE Int. J. Engines 8. https://doi.org/10.4271/2015-24-2443

Bešenić, T., Baleta, J., Pachler, K., Vujanović, M., 2020. Numerical modelling of sulfur dioxide absorption for spray scrubbing. Energy Convers. Manag. 217, 112762. https://doi.org/10.1016/j.enconman.2020.112762

Bešenić, T., Mikulčić, H., Vujanović, M., Duić, N., 2018. Numerical modelling of emissions of nitrogen oxides in solid fuel combustion. J. Environ. Manage. 215, 177–184. https://doi.org/10.1016/J.JENVMAN.2018.03.014

Bohlooli Arkhazloo, N., Bouissa, Y., Bazdidi-Tehrani, F., Jadidi, M., Morin, J.-B., Jahazi, M., 2019. Experimental and unsteady CFD analyses of the heating process of large size forgings in a gas-fired furnace. Case Stud. Therm. Eng. 14, 100428. https://doi.org/10.1016/j.csite.2019.100428

Boulet, P., Collin, A., Consalvi, J.L., 2007. On the finite volume method and the discrete ordinates method regarding radiative heat transfer in acute forward anisotropic scattering media. J. Quant. Spectrosc. Radiat. Transf. 104, 460–473. https://doi.org/10.1016/j.jqsrt.2006.09.010

Cassol, F., Brittes, R., Centeno, F.R., da Silva, C.V., França, F.H.R., 2015. Evaluation of the gray gas model to compute radiative transfer in non-isothermal, non-homogeneous participating medium containing CO2, H2O and soot. J. Brazilian Soc. Mech. Sci. Eng. 37, 163–172. https://doi.org/10.1007/s40430-014-0168-5

Cernat, A., Pana, C., Negurescu, N., Lazaroiu, G., Nutu, C., 2015. Aspects of the animal fat use at the diesel engine fuelling. Proc. Univ. Power Eng. Conf. 1–6. https://doi.org/10.1109/UPEC.2015.7339917

Cerutti, M., Andreini, A., Facchini, B., Mangani, L., 2008. Modeling of turbulent combustion and radiative heat transfer in a object-oriented cfd code for gas turbine application, in: Proceedings of the ASME Turbo Expo. pp. 809–822. https://doi.org/10.1115/GT2008-51117

Chai, J.C., Lee, H.S., Patankar, S. V., 1994. Finite Volume Method for Radiation Heat Transfer. J. Thermophys. Heat Transf. 8, 419–425. https://doi.org/10.2514/3.559

Chai, J.C., Parthasarathy, G., Lee, H.S., Patankar, S. V., 1995. Finite volume radiative heat transfer procedure for irregular geometries. J. Thermophys. Heat Transf. 9, 410–415. https://doi.org/10.2514/3.682

Coelho, P.J., 2018. Radiative Transfer in Combustion Systems, in: Handbook of Thermal Science and Engineering. Springer International Publishing, Cham, pp. 1173–1199. https://doi.org/10.1007/978-3-319-26695-4_61

Coelho, P.J., 2014a. Advances in the discrete ordinates and finite volume methods for the solution of radiative heat transfer problems in participating media. J. Quant. Spectrosc. Radiat. Transf. 145, 121–146. https://doi.org/10.1016/j.jqsrt.2014.04.021

Coelho, P.J., 2014b. Advances in the discrete ordinates and finite volume methods for the solution of radiative heat transfer problems in participating media. J. Quant. Spectrosc. Radiat. Transf. 145, 121–146. https://doi.org/10.1016/j.jqsrt.2014.04.021

Coelho, P.J., 2013. on the Convergence of the Discrete Ordinates and Finite Volume Methods for the Solution of the Radiative Transfer Equation M.

Colin, O., Benkenida, A., 2004. The 3-zones Extended Coherent Flame Model (ECFM3Z) for computing premixed/diffusion combustion. Oil Gas Sci. Technol. 59, 593–609. https://doi.org/10.2516/ogst:2004043

Dec, J.E., 2009. Advanced compression-ignition engines—understanding the in-cylinder processes. Proc. Combust. Inst. 32, 2727–2742. https://doi.org/10.1016/j.proci.2008.08.008

Dorigon, L.J., Duciak, G., Brittes, R., Cassol, F., Galarça, M., França, F.H.R., 2013. WSGG correlations based on HITEMP2010 for computation of thermal radiation in non-isothermal, non-homogeneous H2O/CO2 mixtures. Int. J. Heat Mass Transf. 64, 863–873. https://doi.org/10.1016/j.ijheatmasstransfer.2013.05.010

Dua, S.S., Ping, C., 1975. Multi-dimensional radiative transfer in non-isothermal cylindrical media with non-isothermal bounding walls. Int. J. Heat Mass Transf. 18, 245–259. https://doi.org/10.1016/0017-9310(75)90157-X

E, J., Pham, M., Zhao, D., Deng, Y., Le, D.H., Zuo, W., Zhu, H., Liu, T., Peng, Q., Zhang, Z., 2017. Effect of different technologies on combustion and emissions of the diesel engine fueled with biodiesel: A review. Renew. Sustain. Energy Rev. https://doi.org/10.1016/j.rser.2017.05.250

Fajri, H.R., Jafari, M.J., Shamekhi, A.H., Jazayeri, S.A., 2017. A numerical investigation of the effects of combustion parameters on the performance of a compression ignition engine toward NOx emission reduction. J. Clean. Prod. 167, 140–153. https://doi.org/10.1016/j.jclepro.2017.08.146

Fernandez, S.F., Paul, C., Sircar, A., Imren, A., Haworth, D.C., Roy, S., Modest, M.F., 2018. Soot and spectral radiation modeling for high-pressure turbulent spray flames. Combust. Flame 190, 402–415. https://doi.org/10.1016/j.combustflame.2017.12.016

Fiveland, W.A., 1984. Discrete-Ordinates Solutions of the Radiative Transport Equation for Rectangular Enclosures. J. Heat Transfer 106, 699. https://doi.org/10.1115/1.3246741

Gao, H., Li, X., Xue, J., Bai, H., He, X., Liu, F., 2016. A modification to the WAVE breakup model for evaporating diesel spray. Appl. Therm. Eng. 108, 555–566. https://doi.org/10.1016/j.applthermaleng.2016.07.152

Granate, P., Coelho, P.J., Roger, M., 2016. Radiative heat transfer in strongly forward scattering media using the discrete ordinates method. J. Quant. Spectrosc. Radiat. Transf. 172, 110–120. https://doi.org/10.1016/j.jqsrt.2015.12.011

Guan, B., Zhan, R., Lin, H., Huang, Z., 2015. Review of the state-of-the-art of exhaust particulate filter technology in internal combustion engines. J. Environ. Manage. 154, 225–258. https://doi.org/10.1016/j.jenvman.2015.02.027

Gupta, A., Mishra, P.C., 2019. Optimization of emission characteristics of spark ignition engine with chambered straight muffler running in methanol blend:An engine development technique for environmental sustainability. J. Clean. Prod. 238. https://doi.org/10.1016/j.jclepro.2019.117778

Hanjalić, K., Popovac, M., Hadžiabdić, M., 2004. A robust near-wall elliptic-relaxation eddy-viscosity turbulence model for CFD. Int. J. Heat Fluid Flow 25, 1047–1051. https://doi.org/10.1016/j.ijheatfluidflow.2004.07.005

Honus, S., Pospíšilík, V., Jursová, S., Šmída, Z., Molnár, V., Dovica, M., 2017. Verifying the Prediction Result Reliability Using k-ε, Eddy Dissipation, and Discrete Transfer Models Applied on Methane Combustion Using a Prototype Low-Pressure Burner. Adv. Sci. Technol. Res. J. 11, 252–259. https://doi.org/10.12913/22998624/80922

Jurić, F., Petranović, Z., Vujanović, M., Katrašnik, T., Vihar, R., Wang, X., Duić, N., 2019. Experimental and numerical investigation of injection timing and rail pressure impact on combustion characteristics of a diesel engine. Energy Convers. Manag. 185, 730–739. https://doi.org/10.1016/j.enconman.2019.02.039

Kun-Balog, A., Sztankó, K., Józsa, V., 2017. Pollutant emission of gaseous and liquid aqueous bioethanol combustion in swirl burners. Energy Convers. Manag. 149, 896–903. https://doi.org/10.1016/j.enconman.2017.03.064

Lamas, M.I., Rodríguez, J. de D., Castro-Santos, L., Carral, L.M., 2019. Effect of multiple

injection strategies on emissions and performance in the Wärtsilä 6L 46 marine engine. A numerical approach. J. Clean. Prod. 206, 1–10. https://doi.org/10.1016/j.jclepro.2018.09.165

Lazaroiu, G., Pană, C., Mihaescu, L., Cernat, A., Negurescu, N., Mocanu, R., Negreanu, G., 2017. Solutions for energy recovery of animal waste from leather industry. Energy Convers. Manag. 149, 1085–1095. https://doi.org/10.1016/j.enconman.2017.06.042

López, José J., García-Oliver, J.M., García, A., Villalta, D., 2019. Development of a soot radiation model for diesel flames. Appl. Therm. Eng. https://doi.org/10.1016/j.applthermaleng.2019.04.120

López, J Javier, García, A., Monsalve-serrano, J., Cogo, V., Wittek, K., 2019. Potential of a two-stage variable compression ratio downsized spark ignition engine for passenger cars under different driving conditions. Energy Convers. Manag. 112251. https://doi.org/10.1016/j.enconman.2019.112251

Mikulčić, H., Baleta, J., Klemeš, J.J., 2020. Sustainability through combined development of energy, water and environment systems. J. Clean. Prod. https://doi.org/10.1016/j.jclepro.2019.119727

Mikulčić, H., Klemeš, J.J., Duić, N., 2016. Shaping sustainable development to support human welfare. Clean Technol. Environ. Policy 18, 1633–1639. https://doi.org/10.1007/s10098-016-1269-x

Mishra, S.C., Chugh, P., Kumar, P., Mitra, K., 2006. Development and comparison of the DTM, the DOM and the FVM formulations for the short-pulse laser transport through a participating medium. Int. J. Heat Mass Transf. 49, 1820–1832. https://doi.org/10.1016/j.ijheatmasstransfer.2005.10.043

Mobasheri, R., 2015. Analysis the ECFM-3Z Combustion Model for Simulating the Combustion Process and Emission Characteristics in a HSDI Diesel Engine. Int. J. Spray Combust. Dyn. 7, 353–371. https://doi.org/10.1260/1756-8277.7.4.353

Modest, M.F., 2013. Radiative Heat Transfer, 3rd ed, Elsevier. Elsevier. https://doi.org/10.1016/B978-0-12-503163-9.X5000-0

Modest, M.F., Haworth, D.C., 2016. Radiative heat transfer in high-pressure combustion systems, in: SpringerBriefs in Applied Sciences and Technology. Springer Verlag, pp. 137–148. https://doi.org/10.1007/978-3-319-27291-7_7

Pang, K.M., Karvounis, N., Walther, J.H., Schramm, J., 2016. Numerical investigation of soot formation and oxidation processes under large two-stroke marine diesel engine-like conditions using integrated CFD-chemical kinetics. Appl. Energy 169, 874–887. https://doi.org/10.1016/j.apenergy.2016.02.081

Pang, K.M., Ng, H.K., Gan, S., 2012. Investigation of fuel injection pattern on soot formation and oxidation processes in a light-duty diesel engine using integrated CFD-reduced

chemistry. Fuel 96, 404–418. https://doi.org/10.1016/j.fuel.2012.01.002

Paul, C., Ferreyro Fernandez, S., Haworth, D.C., Roy, S., Modest, M.F., 2019. A detailed modeling study of radiative heat transfer in a heavy-duty diesel engine. Combust. Flame 200, 325–341. https://doi.org/10.1016/j.combustflame.2018.11.032

Petranović, Z., Bešenić, T., Vujanović, M., Duić, N., 2016. Modelling pollutant emissions in diesel engines, influence of biofuel on pollutant formation. J. Environ. Manage. 1–9. https://doi.org/10.1016/j.jenvman.2017.03.033

Petranović, Z., Vujanović, M., Duić, N., 2015. Towards a more sustainable transport sector by numerically simulating fuel spray and pollutant formation in diesel engines. J. Clean. Prod. 88, 272–279. https://doi.org/10.1016/j.jclepro.2014.09.004

Rao, V., Honnery, D., 2013. A comparison of two NO x prediction schemes for use in diesel engine thermodynamic modelling. Fuel 107, 662–670. https://doi.org/10.1016/j.fuel.2013.01.071

Soni, D.K., Gupta, R., 2017. Numerical analysis of flow dynamics for two piston bowl designs at different spray angles. J. Clean. Prod. 149, 723–734. https://doi.org/10.1016/j.jclepro.2017.02.142

Sremec, M., Taritaš, I., Sjerić, M., Kozarac, D., 2017. Numerical Investigation of Injection Timing Influence on Fuel Slip and Influence of Compression Ratio on Knock Occurrence in Conventional Dual Fuel Engine. J. Sustain. Dev. Energy, Water Environ. Syst. 5, 518–532. https://doi.org/10.13044/j.sdewes.d5.0163

Stančin, H., Mikulčić, H., Wang, X., Duić, N., 2020. A review on alternative fuels in future energy system. Renew. Sustain. Energy Rev. 128, 109927. https://doi.org/10.1016/j.rser.2020.109927

Taghavifar, Hadi, Taghavifar, Hamid, Mardani, A., Mohebbi, A., Khalilarya, S., Jafarmadar, S., 2016. Appraisal of artificial neural networks to the emission analysis and prediction of CO2, soot, and NOx of n-heptane fueled engine. J. Clean. Prod. 112, 1729–1739. https://doi.org/10.1016/j.jclepro.2015.03.035

Tatschl, R., 2012. Appendix 3D-CFD Simulation of IC-Engine Flow, Mixture Formation and Combustion with AVL FIRE, Combustion Engines Development. https://doi.org/10.1007/978-3-642-14094-5

Vujanović, M., Duić, N., Tatschl, R., 2009. Validation of reduced mechanisms for nitrogen chemistry in numerical simulation of a turbulent non-premixed flame. React. Kinet. Catal. Lett. 96, 125–138. https://doi.org/10.1007/s11144-009-5463-2

Wu, S., Zhou, D., Yang, W., 2019. Implementation of an efficient method of moments for treatment of soot formation and oxidation processes in three-dimensional engine simulations. Appl. Energy 254. https://doi.org/10.1016/j.apenergy.2019.113661

Yildiz, I., Açıkkalp, E., Caliskan, H., Mori, K., 2019. Environmental pollution cost analyses

of biodiesel and diesel fuels for a diesel engine. J. Environ. Manage. 243, 218–226. https://doi.org/10.1016/j.jenvman.2019.05.002

Yoshikawa, T., Reitz, R.D., 2009. Effect of Radiation on Diesel Engine Combustion and Heat Transfer. J. Therm. Sci. Technol. 4, 86–97. https://doi.org/10.1299/jtst.4.86

Yue, Z., Reitz, R.D., 2019. Numerical investigation of radiative heat transfer in internal combustion engines. Appl. Energy 235, 147–163. https://doi.org/10.1016/j.apenergy.2018.10.098